 doi:10.20944/preprints202205.0201.v1

Article

A label-free cell sorting approach to highlight the impact of intratumoral cellular heterogeneity and cancer stem cells on response to therapies.

Céline Hervieu [1], Mireille Verdier [1], Gaëlle Bégaud [1], Niki Christou [1,2], Magali Sage [3], Julie Pannequin [4], Serge Battu [1,†] and Muriel Mathonnet [1,2,*,†]

[1] UMR INSERM 1308-CAPTuR "Control of Cell Activation in Tumor Progression and Therapeutic Resistance", Faculty of Medicine, Ω-Health Institute, University of Limoges, 87025 Limoges CEDEX, France; celine.hervieu@unilim.fr, mireille.verdier@unilim.fr, gaelle.begaud@unilim.fr, niki.christou@unilim.fr, serge.battu@unilim.fr, muriel.mathonnet@unilim.fr

[2] Department of General, Endocrine and Digestive Surgery, University Hospital of Limoges, 87025 Limoges CEDEX, France

[3] BISCEm US42 INSERM / UAR 2015 CNRS "Integrative Biology Health Chemistry Environment", Ω-Health Institute, 87025 Limoges CEDEX, France; magali.sage@unilim.fr.

4 UMR 5203 CNRS, INSERM, Institute of Functional Genomics, University of Montpellier, Montpellier, France; julie.pannequin@igf.cnrs.fr.

* Correspondence: muriel.mathonnet@unilim.fr

† These authors equally contributed to this work.

Abstract: Cancer stem cells play a crucial role in tumor initiation, metastasis and therapy resistance. Cellular heterogeneity and plasticity challenge the isolation of cancer stem cells. The impact of intratumoral cellular heterogeneity in the context of treatment resistance using a label-free approach remains understudied. Here, we use the sedimentation field-flow fractionation technique to separate, without labeling, cell subpopulations of colorectal cancer cell lines and primary cultures according to their biophysical properties. One of the three cell subpopulations sorted by SdFFF exhibits cancer stem cell traits, including high tumorigenicity in vivo, and a higher frequency of tumor-initiating cells compared to the other subpopulations. In vitro two- and three-dimensional chemosensitivity assays emphasize the therapeutic relevance of this cancer stem cell-like subpopulation due to its chemoresistance. Therefore, our findings highlight a label-free cell sorting approach to reveal intratumoral cellular heterogeneity and its implication in therapy resistance. This approach enables the study of the individualized response of each sorted cell subpopulation by breaking down the tumor, thus offering new perspectives for personalized therapy.

Keywords: cancer stem cells; colorectal cancer; label-free cell sorting; chemoresistance; intratumoral cellular heterogeneity.

1. Introduction

Despite therapeutic advances, colorectal cancer (CRC) remains a major cause of mortality worldwide [1]. Early diagnosis plays a crucial role in the survival of CRC patients. At diagnosis, patients with localized CRC represent 37% of cases, while those with metastatic stage account for 22%, based on the Surveillance, Epidemiology, and End Results (SEER) program [1]. Importantly, five-year survival is strongly related to CRC stage. Indeed, the 5-year survival is around 90% for localized CRC, whereas it decreases sharply for metastatic CRC with only 14% survival. A better understanding of the cells responsible for CRC progression, metastasis and treatment resistance is required. Although new treat-

 doi:10.20944/preprints202205.0201.v1

ment options are available, chemotherapy remains a standard therapy for CRC after surgery [2]. Treatment regimens for patients with localized or advanced CRC include 5-fluorouracil (5-FU)-based chemotherapies, such as FOLFOX (5-FU, leucovorin, and oxaliplatin) or FOLFIRI (5-FU, leucovorin, and irinotecan) or FOLFIRINOX (5-FU, leucovorin, oxaliplatin and irinotecan) [3,4]. Therapeutic resistance and relapse are responsible for decreased 5-year survival in advanced CRC. One explanation for therapy failure is the presence of a minor cell subpopulation, cancer stem cells (CSCs), which are resistant to conventional therapies and therefore likely to cause tumor relapse [5]. CSCs are a small population of cancer cells endowed with self-renewal, multi-lineage differentiation, and tumor-initiating capacity in immunocompromised mice [6,7]. The main challenge for CSC study is their identification and isolation. Surface markers were originally and for a long time used to identify CSCs. However, due to CSC plasticity and the shared expression of certain markers by intestinal stem cells or cancer cells, the use of markers is no longer sufficient to define a CSC [8,9]. Nowadays, functional characteristics such as tumorigenic potential, relative quiescence and chemoresistance are more often used to identify CSCs. The CSC state is subject to cellular plasticity and is inherent to intratumoral cellular heterogeneity. A few years ago, our laboratory adapted the sedimentation field-flow fractionation (SdFFF) technique to separate cell subpopulations of cell lines [10]. SdFFF is a gentle, non-invasive method that does not require cell labeling or fixation [10]. Cell separation by SdFFF depends on the differential elution of cells subjected to both the action of a parabolic profile generated by the mobile phase in the channel and a multi-gravitational external field generated by the channel rotation [9]. Cell separation is based on their biophysical properties such as size and density using the hyperlayer elution mode of SdFFF [11].

In a previous work, our laboratory used SdFFF as a tool to isolate cell subpopulations independently of surface marker expression from CRC cell lines [10]. The results showed that one of the cell subpopulations sorted by SdFFF exhibited CSC-like features in two early-stage CRC cell lines [10,12]. However, the ability of this cell subpopulation to initiate tumors in mice, which is the gold standard for defining a CSC, remains to be determined. In our study, we therefore pursued phenotypic and functional characterization of the sorted cell subpopulations and evaluated their ability to generate tumors in vivo. Furthermore, due to the involvement of CSCs in tumor progression and metastasis, we performed these experiments using late-stage CRC cell lines, in addition to early-stage ones, as well as primary cultures. Finally, as CSCs play a key role in resistance to conventional therapies, we explored the response of SdFFF-sorted cell subpopulations to chemotherapies. Thus, our study aims to highlight the impact of intratumoral cellular heterogeneity in the context of treatment resistance in order to provide leads for a more personalized therapy. In agreement with previous results, we report here that SdFFF-sorted cell subpopulations have distinct phenotypic and functional characteristics [10]; nevertheless, in our study CSC marker expression does not necessarily correlate with CSC functional characteristics. Characterization results show that a cell subpopulation exhibits CSC functional hallmarks, including in vivo tumorigenicity and resistance to conventional therapies, for both early- and late-stage cell lines as well as for primary cultures. Therefore, we highlighted a label-free cell sorting approach to unravel intratumoral cellular heterogeneity and identify chemoresistance from the individualized response of each sorted cell subpopulation. In fine, this approach could provide valuable information from CRC patient samples, thus offering new perspectives for more personalized therapy.

2. Materials and Methods

Cell cultures

Four colorectal cancer cell lines were used. The two early stage CRC cell lines, WiDr (CCL-218™) and SW480 (CCL-228™), and the metastatic ones, SW620 (CCL-227™) and T84 (CCL-248™), were obtained from the American Type Culture Collection (ATCC/LGC

 doi:10.20944/preprints202205.0201.v1

Promochem, France). SW480 and SW620 were established from the same patient, SW480 is from the patient's primary tumor while SW620 is from lymph node metastases. T84 cell line is derived from lung metastasis of a CRC patient. Cells were maintained at 37 °C under humidified 5% CO_2 in MEM medium (#31095-029, Gibco™) for WiDr and RPMI GlutaMAX medium (#61870-010, Gibco™) for SW480, SW620 and T84 cell lines, both supplemented with 10% foetal bovine serum (FBS), 1 mM sodium pyruvate (#11360-039, Gibco™), 100 IU/ml penicillin and 100 mg/ml streptomycin (#15140-122, Gibco™), and only for WiDr 1% non-essential amino acids (#11140-035, Gibco™) [13].

Two primary cultures from CRC patients (CPP14 and CPP35) were obtained from the Institute of Functional Genomics (Univ. Montpellier, CNRS, INSERM, Montpellier, France), after informed consent of patients (Material Transfer Agreement CNRS 190287). The primary culture CPP14 is derived from a patient with T2N0M0 CRC, i.e. early stage (stage I), while CPP35 is derived from a patient with T4aN0M0 CRC, i.e. a stage at which the tumor has invaded the peritoneum (stage IIB), as indicated in Table 1 [14]. Both primary cultures are treatment-naive. The culture conditions for these primary cultures are DMEM GlutaMAX medium (#61965059, Gibco™) supplemented with 10% FBS, 100 IU/mL penicillin and 100 mg/mL streptomycin, at 37°C under a humidified atmosphere of 5% CO_2.

Table 1. Clinical data from colorectal cancer patients from whom primary cultures were established.

Primary cultures	CPP14	CPP35
pTNM	T2N0M0 Early-stage tumor	T4aN0M0 Tumor-invaded peritoneum
Stages	Stage I	Stage IIb
Primary location	Left colon	Transverse colon
Chemotherapy	No	No
Radiotherapy	No	No
Curative surgery	Yes	Yes

SdFFF cell sorting

The SdFFF technique used enables sorting of cell subpopulations as previously described and schematized [9,10]. Cell-solid phase interactions in SdFFF are limited due to the use of a ribbon-like empty channel with no stationary phase and a size/density-based separation mechanism through the hyperlayer elution mode. SdFFF parameters used during cell sorting are field (units of gravity, g), flow rate of the mobile phase which is sterile phosphate-buffered saline (PBS, #14190-094, Gibco™) and the rotation speed of the channel (revolutions per minute, rpm) which is related to the field. Adjustment steps were performed in order to choose the SdFFF parameters allowing a correct separation between the dead volume peak and the peak containing the cells, and to define the best elution conditions for the different cell lines and primary cultures used. The elution conditions are summarized in Table 2, with the parameters checked before and during each cell sorting.

Table 2. Optimal elution condition for cell sorting of CRC cell lines and primary cultures by SdFFF.

Cell lines and primary cultures	Cell concentrations (cells/mL)	Field (g)	Flow rate (mL/min)
WiDr	$2x10^6$	8	0.8
SW480	$2.5x10^6$	8	0.8
SW620	$2.5x10^6$	8	0.8
T84	$3x10^6$	15	0.8
CPP14	$2.5x10^6$	10	0.8
CPP35	$2.5x10^6$	8	1

 doi:10.20944/preprints202205.0201.v1

The injected volume of the cell suspension, 100µL, as well as the detection wavelength, 254nm, are common for each cell line and primary culture. A cleaning and decontamination procedure is performed at the end of each cell sorting [15]. Once sorted, cells can be recultured in vitro and characterized, as no cell fixation or labeling is required for SdFFF. In order to perform experiments with the sorted cells, successive injections and collections of the same cell suspension are required to obtain a sufficient quantity of cells.

CSC marker expression

After cell sorting by SdFFF, cell subpopulation concentrations were standardized to the same amount of cells in each condition. Anti-CD44, anti-LGR5, anti-CD133/1 and viability marker antibodies were added to the cells and incubated for 30 minutes at 4°C and in the dark, antibody references are summarized in Table S1. The viability marker was used to exclude nonviable cells. Cells were then fixed in 4% paraformaldehyde (PFA, #10231622, Fischer Scientific) for 10 minutes at room temperature and permeabilized with Perm Buffer III (#558050, BD Phosflow™) for 30 minutes at 4°C. Next, antibodies recognizing the intracellular marker BMI-1 were added and incubated for 30 minutes at 4°C in the dark (reference in Table S1). As reference controls, anti-IgG2bκ FITC, anti-IgG2bκ PE-Vio 770, anti-IgG1 PE-Vio 615 and mouse anti-IgG1κ PE isotype controls were used under the same conditions and concentrations to ensure specific recognition of our antibodies of interest and to set gates (references in Table S1). Samples were analyzed by the CytoFlex LX and data analysis using Kaluza software.

Cell cycle analysis

Cell concentrations of SdFFF-sorted subpopulations were standardized in each condition. After a centrifugation step, the cells were resuspended with cold PBS, fixed with cold 96% ethanol added slowly and under shaking, and then placed at -20°C. After a few minutes at room temperature, the cells were washed and then resuspended with PBS and RNAse A (#R6148, Sigma-Aldrich) for 20 minutes at room temperature. Next, propidium iodide was added 15 minutes before acquisition on the FACS Calibur. Data analysis was performed with ModFit LT™ software.

Clonogenic assay: soft agar assay

This assay is based on the use of two gels, the first is a 0.5% agar gel that prevents the cells from adhering to the culture plate and the second is a 0.7% agarose gel containing the cells. The agar (#A7002, Sigma-Aldrich) and agarose (#A9539, Sigma-Aldrich) solutions were prepared upstream with sterile PBS and autoclaved to limit potential contamination. Agar gel was prepared in advance and plated into wells of 24-well plates at room temperature and under the culture hood. Once agar gel solidified, the agarose gel was heated and then gently mixed with cell subpopulations sorted by SdFFF to have a cell concentration of $1x10^3$ cells per well (12 wells/condition). As soon as the second gel solidified, culture medium was added on top to prevent evaporation and 24-well culture plates were incubated at 37°C under a humidified atmosphere of 5% CO_2 for 30 days. Four weeks later, the formed colonies were fixed in 4% PFA (#10231622, Fischer Scientific) for 15 minutes and then stained with 0.1% crystal violet. Wells of the 24-well plates used were captured with the Leica DFC300 FX Digital Color Camera to allow colony quantification and analyzed by ImageJ software.

In vivo tumor initiation assay

SdFFF-sorted cell subpopulations of the WiDr cell line were injected subcutaneously into nude mice (Hsd:Athymic Nude-Foxn1nu nu/nu, 6 weeks old, female, five mice per group) in decreasing amounts of cells (1000, 500, and 100) in Matrigel (#356237, Corning)-MEM medium (v:v). Mice weight and tumor size was measured three times a week for 7 weeks. After 50 days, mice were sacrificed and tumors were collected. The number of tumor-bearing mice with a tumor volume greater than $100mm^3$ was counted. The online software Extreme limiting dilution analysis (ELDA) was used from the in vivo results to determine the frequency of tumor occurrence and thus tumor initiating cells frequency

 doi:10.20944/preprints202205.0201.v1

(https://bioinf.wehi.edu.au/software/elda/) [16]. This animal experimentation protocol has been approved by the Ethics Committee for Animal Experimentation n°33 and by the French Ministry of Higher Education, Research and Innovation.

Cytotoxicity assay

To compare results between cell lines, we defined the same cell concentration for all cell lines: 1.5x10^3 cells per well of 96-well plate, after optimization. Once sorted and seeded, cells were then treated for 72 hours with 5-FU (provided by the anticancer preparation unit of the University Hospital of Limoges) using a range from 0.16 to 250µM. Three days later, the MTS reagent was added according to the manufacturer's instructions (#G3580, CellTiter96 AQueous One solution Cell Poliferation assay, Promega) and incubated for 3 hours at 37°C under a humidified atmosphere of 5% CO_2. Absorbance was then measured at 490nm with the Multiskan™ FC 96-well plate reader (Thermo scientific™) and the results were expressed as a percentage comparing the treated condition to the untreated condition defined as 100%. Generation of drug response curves and determination of IC50 values were performed using GraphPad Prism software. We compared the obtained IC50s with those reported at https://www.cancerrxgene.org/.

Proliferation assay

Once sorted by SdFFF, cells were seeded at the same concentration as for the MTS assay, 1.5x10^3 cells per well in 96-well plates. Cells were then treated for 72 hours with the average IC50 values obtained for 5-FU from the cell lines and primary cultures used. Cell proliferation was assessed using the BrdU cell proliferation assay kit (#6813, Cell signaling technology) according to the manufacturer's instructions. Absorbance was then measured at 450nm with the Multiskan™ FC 96-well plate reader (Thermo scientific™) and the results were expressed as a ratio comparing the treated condition to the untreated condition defined as 1.

Cell death assay

From the same cell sorting by SdFFF as for the proliferation analysis, an apoptosis analysis was performed. Cell concentration and 5-FU dose and incubation time were the same as for the cell proliferation assay. Apoptosis rate was measured using the Cell Death Detection ELISA^{PLUS} kit (#11774425001, Roche), according to the manufacturer's instructions. Absorbance was then measured at 405nm with the Multiskan™ FC 96-well plate reader (Thermo scientific™) and the results were expressed as a ratio comparing the treated condition to the untreated condition defined as 1.

Tumorsphere assay

Five hundred cells were seeded in nonadherent 96-well culture plates previously coated with a 10% solution of poly-2-hydroxyethylmethacrylate (#P3932, Sigma Aldrich) in 95% ethanol and dried overnight at 56°C [17]. These cells were cultured in defined medium: with serum-free GlutaMAX-DMEM/F12 (#10565018, Gibco™) medium supplemented with 20 ng/ml epidermal growth factor (#PHG0314, Gibco™), 10 ng/ml basic fibroblast growth factor (#PHG0264, Gibco™), 0.3% glucose (#49163, Sigma-Aldrich), 20 µg/ml insulin (#12585-014, Gibco™), 1:100 N2 supplement (#17502-001, Gibco™)[18] and incubated at 37°C in a humidified atmosphere of 5% CO_2 for one week. Seven days later, spheres larger than 50 µm in diameter were counted using the Leica DMi8 microscope. Then, to study chemotherapy response in a 3D culture model, chemotherapies were added after the seven days of incubation that allow colonosphere formation, and incubated for 3 days. Colonospheres were counted three days after treatment, imaged using the Leica DMi8 microscope, and their size was measured using ImageJ software.

Statistical analysis

All bar plots are represented by the mean ± S.E.M. of results obtained from at least three independent experiments. Flow cytometry results were represented as histograms from one representative biological replicate among the three independent experiments

 doi:10.20944/preprints202205.0201.v1

performed (n=3). Significance of results was specified by stars: *p-value < 0.05, **p-value < 0.01, ***p-value < 0.001. The presence of a star without a bar below indicates that the result is significantly different from the control condition: TP. Significance between the three sorted cell subpopulations was represented using the star and a bar below to allow identification of the subpopulations involved in these significantly different results. Non-significance of results is indicated by ns for not significant. Results were analyzed by the Kruskal-Wallis test for clonogenicity assay because the results did not follow a normal distribution, verified using the Shapiro-Wilk test. Chi-squared test was used to identify the frequency of tumor-initiating cells from in vivo experiment results. The one-way ANOVA test was used for all other experiments because the results followed a normal distribution (Shapiro-Wilk test) and the comparison was between the three sorted cell subpopulations and the control. Statistical tests were performed using PAST software, version 2.17c.

3. Results

3.1. SdFFF technique sorts cell subpopulations expressing cancer stem cell markers from colorectal cancer cell lines.

Firstly, we optimized the sorting conditions for the different cell lines used, by modifying the elution parameters such as flow rate and field. The defined parameters are presented in Table 2. Using a hyperlayer elution mode, cells are eluted according to their biophysical properties, mainly their size and density [10,12,19]. This hyperlayer mode elutes the largest cells first and the densest cells last. Thus, the beginning of the elution peak is rather composed of large and low density cells, while the end of the peak contains small and high density cells [10]. Using SdFFF, we isolated three subpopulations of cells: F1, F2, and F3, as shown in the SW480 fractogram in Figure 1A, in addition to the control. The total peak (TP) is a control of cell sorting efficiency, corresponding to all cells eluted by the device from the beginning of the F1 collection to the end of the F3 collection (Figure 1A). Previous studies have shown comparable results between the TP control and the unsorted cell line that underwent the same conditions as the sorted subpopulations, called crude, so we decided to use the TP as a control in our following experiments [10,12]. The cell size of these subpopulations was monitored by a coulter counter and confirmed that the cells eluted first, i.e. F1, are larger than those eluted last, i.e. F3, with results comparable to those published in Mélin et al. [10].

Secondly, we phenotypically characterized these sorted cell subpopulations by analyzing for the first time the expression of CSC markers in the four cell lines by flow cytometry. In the publication of Mélin et al. and until now, the analysis of CSC marker expression from SdFFF-sorted cell subpopulations was only performed by immunofluorescence, which is a less robust and less objective technique than flow cytometry mainly due to the number of cells analyzed [10]. Using flow cytometry, we analyzed the expression of CD44, LGR5, BMI1, and CD133 markers within SdFFF-sorted cell subpopulations of both early-stage CRC cell lines, WiDr and SW480, and metastatic stage cell lines, SW620 and T84 (Figure 1B-F). Isotype controls with fluorochromes identical to our markers of interest were performed under the same experimental conditions to position the gates (Figure S1A). Initially, we compared the expression of these markers in the four cell lines. CSC markers are found in all cell lines but at different expression levels (Figure 1B-F). Looking at the TP values, we notice that LGR5 and CD133 markers are more highly expressed in the early stage cell lines while BMI1 marker expression is higher in the late stage cell lines (Figure 1D-F). CD44 marker expression is comparable between cell lines except for the SW620 cell line that has a lower expression (Figure 1C). Thus, these results show that these CSC markers are expressed in all four cell lines and interestingly, for three of the four markers, the expression levels appear to be correlated with CRC stages.

 doi:10.20944/preprints202205.0201.v1

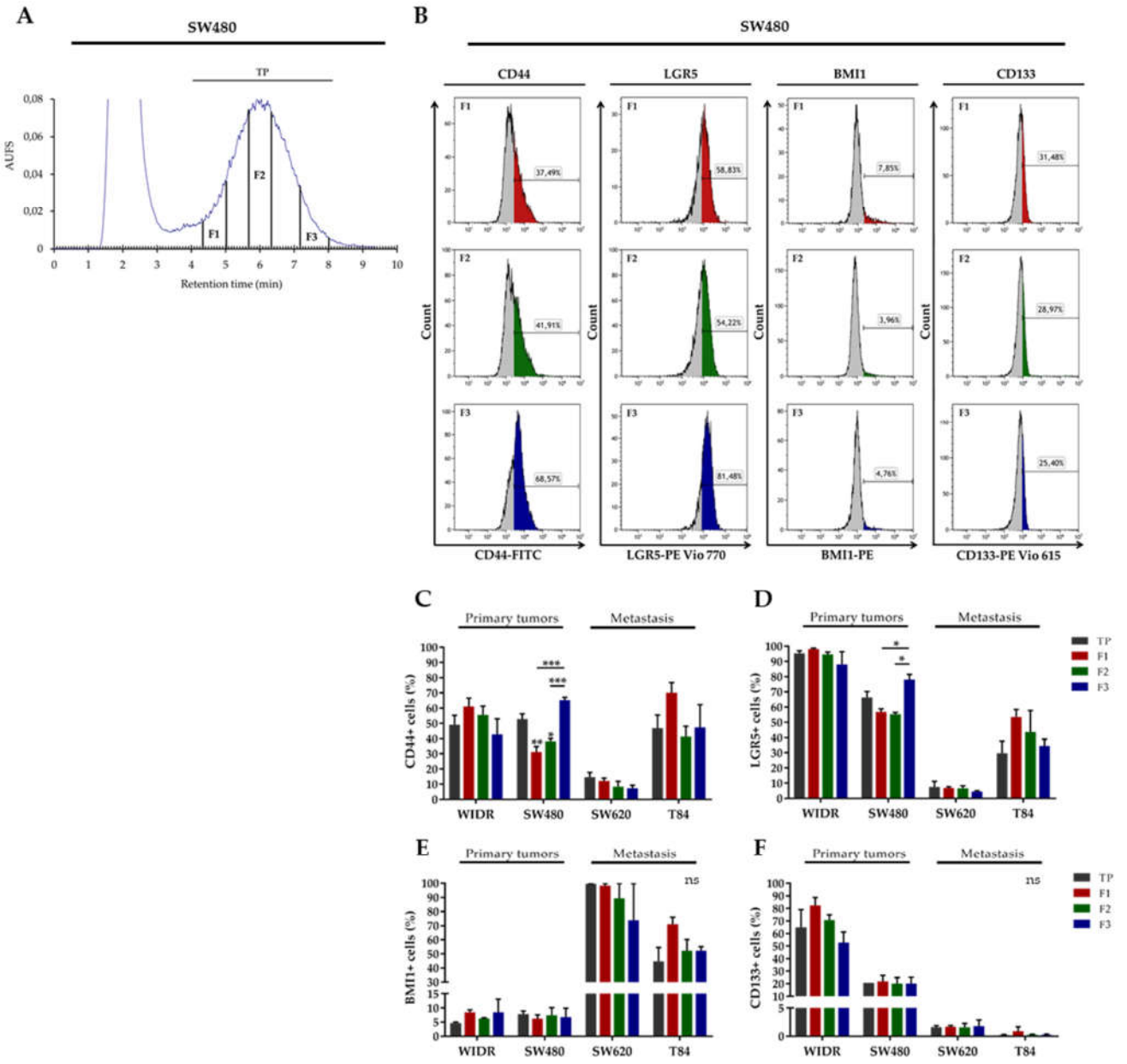

Figure 1. Phenotypic characterization of SdFFF-sorted cell subpopulations from CRC cell lines. (A) Fractogram of the SW480 cell line obtained by SdFFF with the sorted cell subpopulations: total peak control (TP), F1, F2 and F3. AUFS: absorbance units full scale. (B) The expression level of CSC markers, CD44, LGR5, BMI1 and CD133, was assessed by flow cytometry and plotted as histograms for the SW480 cell line. CD44 and LGR5 markers are more expressed in SW480 F3 compared to other subpopulations. Graphs show one representative biological replicate (n=3). (C-F) Quantification of CD44 (C), LGR5 (D), BMI1 (E) and CD133 (F) positive cells was summarized in the bar plot for all cell lines. The results show variable expression levels of CSC markers between the sorted cell subpopulations, with significantly higher expression of the markers LGR5 and CD44 in F3 for SW480 and a trend rather in F1 for WiDr, SW620 and T84. All these results are represented as means ± SEM and statistical differences with ns for not significant, *p-value < 0.05, **p-value < 0.01, ***p-value < 0.001 and *alone for significant results compared to TP using One-way ANOVA test.

 doi:10.20944/preprints202205.0201.v1

Next, we focused on flow cytometry results obtained from SdFFF-sorted cell subpopulations. Figure 1B contains the histograms acquired from the three-sorted subpopulations of the SW480 cell line. F3 subpopulation of SW480 has a significantly higher percentage of CD44-positive and LGR5-positive cells compared to F1 and F2 (Figure 1B-D). For BMI1 and CD133 markers, the expression levels are comparable between the sorted SW480 cell subpopulations (Figure 1E-F). For the WiDr, SW620 and T84 cell lines, the percentage of cells positive for all four markers seems to be higher in F1 compared to the other subpopulations but without significant difference (Figure 1C-F). Thus, flow cytometry results show a non-homogeneous distribution of the expression of these CSC markers in the sorted cell subpopulations of all cell lines. Indeed, the percentage of positive cells for these markers is predominant in F3 for SW480 while the trend seems to be in F1 for the WiDr, SW620 and T84 cell lines (Figure 1B-D).

Therefore, these phenotypic characterization results reveal two subpopulations that appear to be distinct: F1 and F3. Furthermore, we confirmed by these results that cell sorting by SdFFF is not dependent on marker expression, which provides new perspectives to study intratumoral cellular heterogeneity. Finally, phenotypic analysis provides interesting preliminary data on CSCs but needs to be completed by a functional analysis because of CSC plasticity [6,20].

3.2. F3 subpopulation has cancer stem cell functional features in colorectal cancer cell lines.

We further investigated SdFFF-sorted cell subpopulations by analyzing their functional properties. First, we examined the cell cycle distribution of the three cell subpopulations from cell lines by flow cytometry (Figure 2A-B). Comparing the TP values, we notice that the proportion of cells in G0/G1 decreases and seems to be correlated with the evolution of CRC stages (Figure 2B). Indeed, the percentage of cells in G0/G1 was significantly different between WiDr and the other three cell lines, as well as between SW480 and T84 (data not shown). Focusing on the flow cytometry histograms of the WiDr cell line, cells in G0/G1 represent approximately 43% for F1, 62% for F2 and 82% for F3 i.e. an almost two-fold difference from F1, while the percentage of cells in G2/M is approximately 27% for F1, 12% for F2 and 3.5% for F3 i.e. a seven-fold difference from F1 (Figure 2A). Cell proportion in each phase of the cell cycle is summarized in the bar plots (Figure 2B, S1B-C). The bar plot results indicate that the percentage of cells in G0/G1 is statistically different between the three WiDr cell subpopulations (Figure 2A-B). A similar observation could be made for all cell lines; the F3 subpopulation is significantly the one with the highest number of cells in G0/G1 phase (Figure 2B). In contrast, the percentage of cells in G2/M is significantly higher in F1 for all cell lines while the proportion of cells in S phase varies more slightly between cell subpopulations (Figure S1B-C). Therefore, F3 subpopulation appears to be more quiescent or poorly proliferative compared to the other sorted cell subpopulations, which is a feature of CSCs.

Subsequently, we assessed the clonogenic capacity of these SdFFF-sorted cell subpopulations by a soft agar assay (Figure 2C-D). Comparing the TP values, the late-stage cell lines seem to form slightly more colonies than the early-stage ones (Figure 2D). F3 subpopulation of the WiDr cell line produces significantly more colonies than F1 and TP, and a similar trend is observed for the other cell lines (Figure 2D). Interestingly, the colonies formed by the SW620 cell line, which is from the same patient as SW480 but at a more advanced stage, appear to be more numerous and larger than those obtained by SW480 (Figure 2C). Hence, the F3 subpopulation seems to be more clonogenic than F1.

Taken together, these functional characterization results highlight two cell subpopulations that seem to oppose each other: F1 and F3, as observed from the phenotypic characterization. The F3 subpopulation is relatively quiescent and clonogenic, which are features of CSCs, whereas F1 is proliferative and less clonogenic. Based on these results, F2 appears to be an intermediate cell subpopulation between F1 and F3, and we will now focus our study on the F1 and F3 subpopulations.

 doi:10.20944/preprints202205.0201.v1

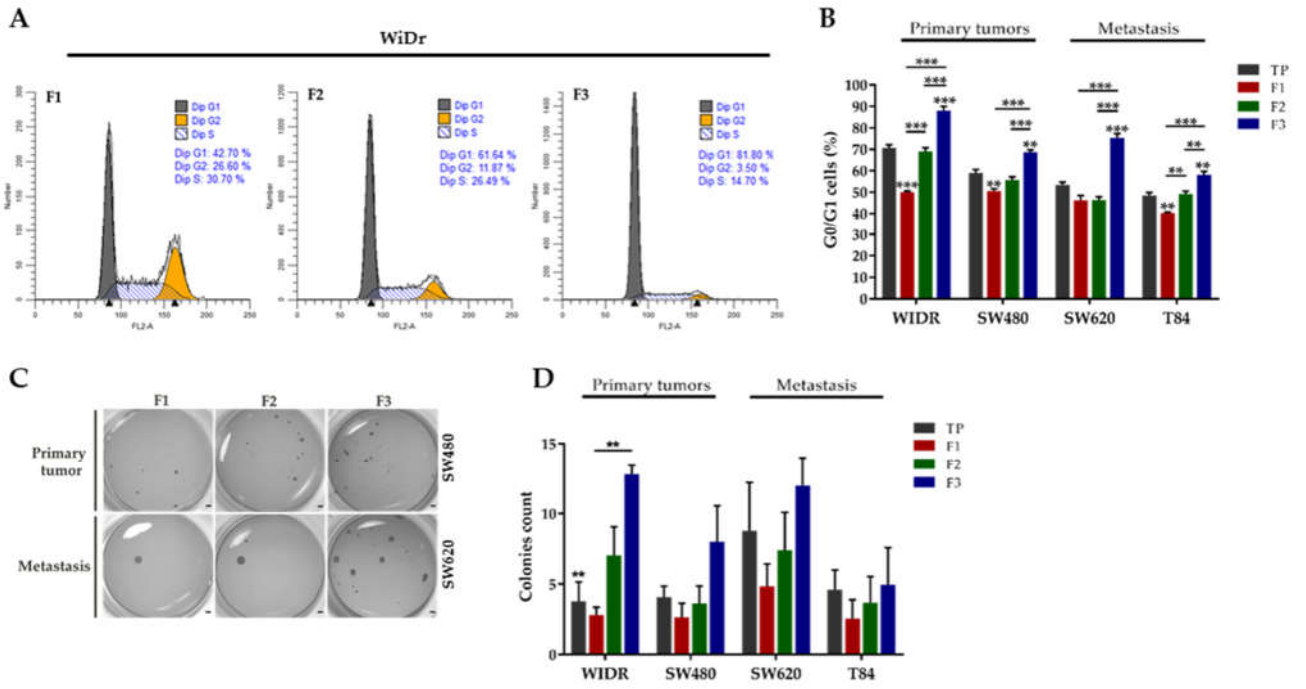

Figure 2. Functional characterization of SdFFF-sorted cell subpopulations from CRC cell lines highlighting a quiescent and clonogenic F3 subpopulation. (A) The distribution of the sorted cell subpopulations in the cell cycle was analyzed by flow cytometry and plotted as histograms using modfit software. The percentage of G0/G1 cells is two-fold higher and seven-fold lower for G2/M cells in the F3 subpopulation compared to F1 for the WiDr cell line. Graphs show one representative biological replicate (n=3). (B) Quantification of G0/G1 cells was performed for each sorted cell subpopulation and cell line, and presented in the bar plot from three biological replicates. For all cell lines, F3 subpopulation has the significantly highest number of cells in G0/G1 compared to the other cell subpopulations. (C-D) Cell clonogenicity was assessed by a soft agar assay. Images of the colonies formed (C) as well as the bar plot (D) show that F3 forms significantly more colonies than F1 for the WiDr cell line with a similar trend for SW480, SW620 and T84. From the colony images, we can notice that the F3 subpopulation of the SW480 and SW620 cell lines appear to form larger colonies compared to F1 and F2. Scale bar 1 mm. All these results are represented as means ± SEM and statistical differences with **p-value < 0.01, ***p-value < 0.001 and *alone for significant results compared to TP using One-way ANOVA test for cell cycle distribution analysis and Kruskal-Wallis test for clonogenicity.

The gold standard test for defining a CSC is the ability to initiate tumors as xenografts in immunocompromised mice [9]. Thus, for the first time, we subcutaneously inoculated the sorted cell subpopulations F1 and F3 at different cell concentrations into athymic nude mice, as illustrated in Figure 3A. We used a single cell line for the in vivo tumor initiation assay in order to meet the guidelines of the 3R rule, and we chose the WiDr cell line on the basis of previous results with the chick chorioallantoic membrane model [12]. The number of tumor-bearing mice with a volume larger than 100 mm^3 was counted seven weeks after injection (Figure 3A). Interestingly, among the 15 mice transplanted with the F1 cell subpopulation only two mice developed tumors compared to eight mice with F3 (Figure 3B). Remarkably, F3 was the only cell subpopulation able to initiate tumor formation at the concentration of 100 injected cells (Figure 3B). Furthermore, F3 is the cell subpopulation with the highest average tumor volume, approximately 450 mm^3 for F3 versus 360 mm^3 for TP and 130 mm^3 for F1, thereby a three-fold difference for F3 compared to F1 (Figure S1D). Importantly, a mean tumor volume above the 100mm3 threshold was obtained between 36 and 39 days for F3 and TP with the 1000 cells injected condition,

Preprints (www.preprints.org) | NOT PEER-REVIEWED | Posted: 16 May 2022 doi:10.20944/preprints202205.0201.v1

whereas it was only reached from 46 days for F1 (Figure S1E). Tumor size can be visualized from the photos of the tumors collected at the end of the experiment in Figure S1F. From these in vivo results, we performed a limiting dilution analysis (LDA) using the extreme LDA software [16]. The frequency of tumor-initiating cells is estimated at one cell in 566 for the F3 subpopulation, compared with one in 3611 for F1. Thus, the frequency is four-fold higher for the F3 subpopulation compared to F1, with a significant p-value (p=0.00886) (Figure 3C). Therefore, F3 subpopulation is more tumorigenic than F1 and has a significantly higher frequency of tumor-initiating cells (Figure 3).

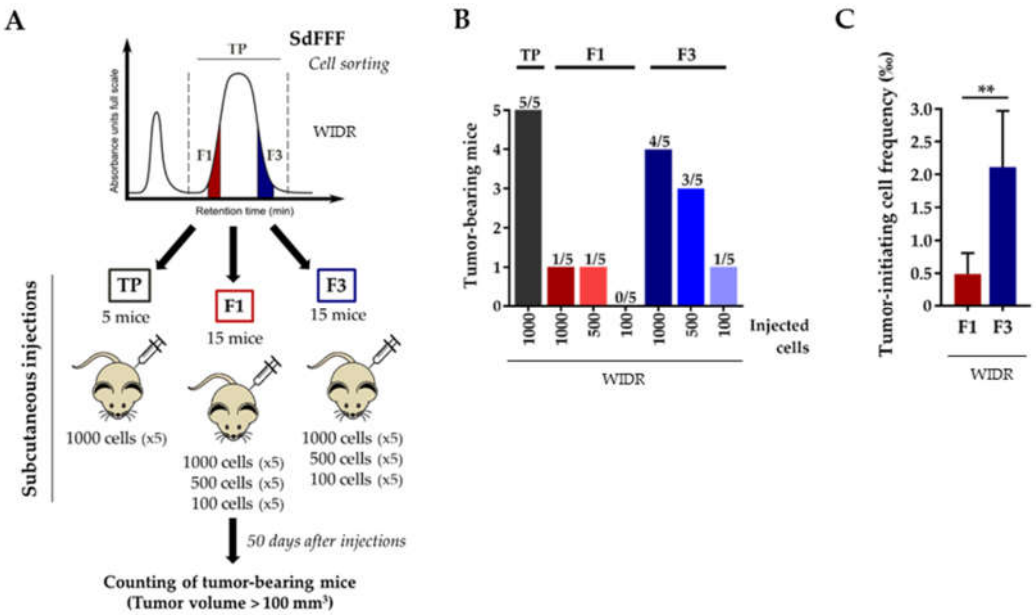

Figure 3. Tumorigenic capacity of the F3 subpopulation in immunodeficient mice, even after an injection of only 100 cells. (A) Schematic representation of the in vivo tumor initiation assay. Nude mice were injected subcutaneously with either 1000, 500 or 100 F1 and F3 cells of the WiDr cell line. (B) The number of tumor-bearing mice (tumor > 100 mm^3) was evaluated 7 weeks after injection and summarized in the bar plot. F3 subpopulation is more tumorigenic than F1, for all cell concentrations. (C) Tumor-initiating cell frequency was determined from in vivo results using extreme limiting dilution analysis (ELDA) software. F3 has a significantly higher frequency of tumor-initiating cells than F1. Results are represented as means ± SEM and statistical differences with **p value < 0.01 using chi-squared test of ELDA software.

Overall, our findings show that SdFFF-sorted cell subpopulations from cell lines exhibit distinct phenotypic and functional characteristics, particularly F1 and F3. Phenotypically, the F3 subpopulation expresses significantly more two of the four studied markers for the SW480 cell line while the expression tends rather in F1 for WiDr, SW620 and T84 (Figure 1). Functional analysis revealed a relatively quiescent, clonogenic and highly tumorigenic cell subpopulation in vivo: F3 (Figure 2 and 3). Thus, the F3 subpopulation exhibits CSC hallmarks including its ability to initiate tumors in vivo and an estimated four-fold higher frequency of tumor-initiating cells than F1 (Figure 3). This subpopulation could therefore be a relevant therapeutic target, which underlines the importance of studying its response to therapies commonly used in CRC treatment.

3.3. F3 subpopulation is resistant to 5-FU in colorectal cancer cell lines.

We then assessed the response to chemotherapy of cell subpopulations sorted by SdFFF. We treated these sorted subpopulations with the most commonly used chemotherapeutic molecule in CRC treatment, 5-FU, and assessed cell viability, proliferation, and apoptosis after treatment, as shown in Figure 4A. First, we applied a dose range of 5-FU

 doi:10.20944/preprints202205.0201.v1

to obtain IC50s for each sorted cell subpopulation and cell line (Figure 4B-C). Comparing the TP values, we notice that the T84 cell line is the most resistant to 5-FU among the four cell lines, with an IC50 of about 13 μM, which may correlate with it being the most advanced cell line (Figure 4C). IC50 values are comparable between the two cell lines SW480 and SW620, and the IC50 of WiDr is approximately 5 μM, which is consistent with the results of the Genomics of Drug Sensitivity in Cancer study (Figure 4C) [21]. Next, focusing on the sorted cell subpopulations, we observe that the F3 subpopulation is significantly more resistant to 5-FU than TP and F1 for the SW480 cell line, with this similar trend for WiDr, SW620 and T84 (Figure 4B-C). Subsequently, we analyzed the impact of 5-FU treatment on cell proliferation. BrdU results show that proliferation is significantly increased after 5-FU treatment in the F3 subpopulation for SW620 and T84 cell lines compared with F1 (Figure 4D). For both early-stage cell lines, proliferation also appears to be higher in the F3 subpopulation in comparison to F1 (Figure 4D). Remarkably, F3 is the only cell subpopulation sorted by SdFFF to show increased proliferation compared to untreated conditions (dashed line). Therefore, 5-FU treatment mainly induces proliferation in the F3 cell subpopulation, whereas in the untreated condition the proliferation rate is higher in F1 (data not shown). In parallel to the proliferation analysis and from the same cell sorting, 5-FU-induced apoptosis was assessed by the cell death ELISA assay. No significant changes are visible between the sorted cell subpopulations for all cell lines (Figure 4E). Thus, these results highlight 5-FU resistance of the F3 subpopulation due to enhanced cell viability and proliferation after treatment (Figure 4).

We also performed these experiments after treatment with oxaliplatin and irinotecan, which are the other two chemotherapies commonly used in the treatment of CRC (Figure S2) [2,9]. The IC50 of oxaliplatin is significantly higher in the F3 subpopulation compared to F1 for the WiDr cell line, with a similar trend for SW480 and SW620 (Figure S2A). Post-treatment cell proliferation appeared to be slightly increased in the F3 subpopulation of these three cell lines compared with F1, without major changes in the apoptosis rate (Figure S2B-C). For the T84 cell line, cell viability is comparable between the sorted cell subpopulations, while proliferation appears to be slightly increased in F3 compared to F1 and apoptosis is significantly decreased in F1 in comparison to F3 (Figure S2A-C). Interestingly, the difference between the F1 and F3 subpopulations of T84 for proliferation and apoptosis rates is equivalent; there is a factor of 1.46 in both cases (Figure S2B-C). Focusing on the results with irinotecan, we note that the IC50 of irinotecan is significantly higher in the F3 subpopulation compared to TP for the T84 cell line, and that this trend is also noticeable for SW480 and SW620 (Figure S2D). Cell proliferation rate after irinotecan treatment appears to be increased in the F3 subpopulation for WiDr, SW480 and T84 cell lines compared to F1 (Figure S2E). Irinotecan-induced apoptosis is significantly decreased in F1 and F3 compared to TP for the T84 cell line, a similar trend is obtained for SW480 (Figure S2F).

Taken together, these results demonstrate that F3 is the most resistant to 5-FU among the cell subpopulations sorted by SdFFF for all cell lines (Figure 4). Similar results were obtained after treatment with oxaliplatin and irinotecan (Figure S2). Resistance to treatment is a fundamental characteristic of CSCs, so these results confirm that the F3 subpopulation has CSC-like properties, especially chemoresistance. These chemosensitivity experiments were performed in a two-dimensional (2D) culture model, however, we are aware that the tumor organization is more complex and this may impact the response to therapy. Thus, we will further investigate the response to therapies using a three-dimensional (3D) culture model.

 doi:10.20944/preprints202205.0201.v1

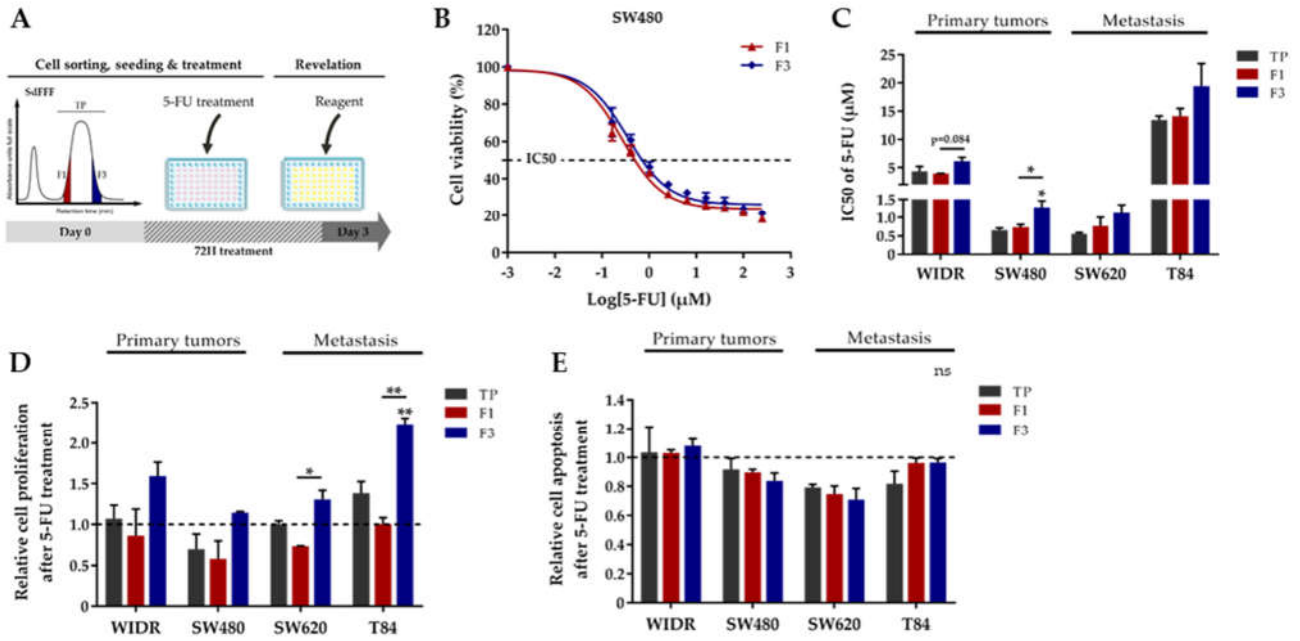

Figure 4. 5-FU resistance of F3 subpopulation from CRC cell lines. (A) Schematic representation of 5-FU response analysis performed. After cell sorting by SdFFF, cell subpopulations were treated with 5-FU for three days and then cell viability, proliferation and apoptosis analysis was performed. (B-C) After 5-FU treatment, cell viability analyzed by MTT assay was presented as a dose-response curve for the SW480 cell line (B) and a bar plot with IC50 values obtained from all cell lines (C). F3 subpopulation has significantly higher cell viability than F1 for the SW480 cell line after treatment, with a similar trend for WiDr, SW620 and T84. (D) Cell proliferation rate after 5-FU treatment was measured by BrdU assay and presented in the bar plot as a ratio between treated and untreated conditions (dashed line). Cell proliferation is significantly increased in F3 compared to F1 for the SW620 and T84 cell lines, with a similar trend for WiDr and SW480. (E) After 5-FU treatment, apoptosis rate was measured using ELISA cell death assay and compared with the untreated condition (dashed line). Apoptosis is comparable between cell subpopulations of all cell lines. All these results are represented as means ± SEM and statistical differences with ns for not significant, *p-value < 0.05, **p-value < 0.01 and *alone for significant results compared to TP using One-way ANOVA test.

3.4. F3 colonospheres are resistant to single and combination chemotherapies in colorectal cancer cell lines.

We next examined the impact of 5-FU-based chemotherapies on the colonospheres from the SdFFF-sorted cell subpopulations. To this end, we performed the sphere formation assay, a 3D cell culture model mimicking tumor organization in vitro. This test relies on the ability of cancer cells to form colonospheres, i.e. microtumor-like spheroids, from a single progenitor cell and is used to assess the tumorigenic potential of solid tumors in vitro [6]. Thus, we sorted and seeded the cell subpopulations in a defined medium for seven days for colonospheres to form, and then treated them with single chemotherapies, as illustrated in Figure 5A. First, all four cell lines have the ability to form colonospheres (Figure 5B). However, colonosphere morphology and size vary between cell lines, with colonosphere size appearing to correlate with the stage of CRC development (Figure 5B). After 5-FU treatment, the number of colonospheres was significantly increased in the F3 subpopulation compared with F1 for both advanced-stage lines, with a similar trend for SW480 (Figure 5C). Colonospheres were also more abundant in the F3 subpopulation than in TP for WiDr after oxaliplatin treatment, with similar observations for SW480 and SW620 (Figure S2G). The same experiment was carried out after treatment with irinotecan and the results showed that F3 was the most resistant of the sorted cell subpopulations for SW480 with a significant difference compared to TP and F1, and similar findings for

 doi:10.20944/preprints202205.0201.v1

SW620 and T84 (Figure S2H). Chemotherapy is most often administered in combination to patients with late-stage CRC, but sometimes also to early-stage patients with risk factors for recurrence [9], in order to potentiate the anticancer effect and prevent recurrence. Accordingly, we evaluated the response of sorted cell subpopulations to chemotherapy combinations, such as FOLFOX, FOLFIRI, and FOLFIRINOX, in addition to the response analysis to single chemotherapies. Combinations of 5-FU-based chemotherapies mainly induce an increase in colonospheres in the F3 subpopulation, with a significant difference between F3 and TP and/or F1 for WiDr after FOLFOX and FOLFIRINOX treatments, as well as for WiDr, SW480 and T84 after FOLFIRI (Figure 5D-F).

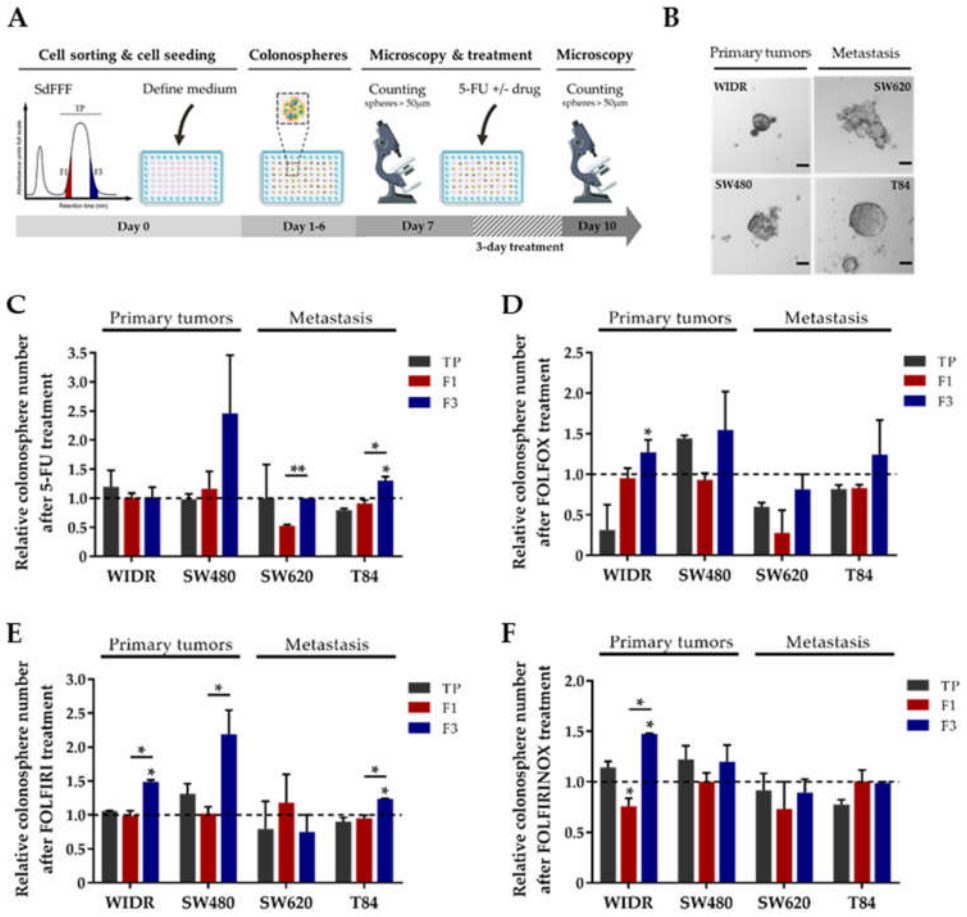

Figure 5. Chemoresistance of F3 colonospheres to 5-FU alone or combined with oxaliplatin and/or irinotecan from CRC cell lines. (A) Schematic representation of chemotherapy response analysis performed from colonospheres. SdFFF-sorted cell subpopulations are seeded at low density in defined medium for seven days and then treated with chemotherapy for three days. Colonospheres with a diameter larger than 50µM are counted before and after treatment. (B) The in vitro tumorigenic potential of cells was assessed by a sphere formation assay. Colonospheres obtained from the different CRC cell lines have distinct morphologies and their size appears to increase with CRC stage. Scale bar 50 µm. (C-F) The impact of chemotherapies on CSC tumorigenic properties in vitro was analyzed after treatment with 5-FU alone (C) or combined with either oxaliplatin (FOLFOX) (D), irinotecan (FOLFIRI) (E), or both (FOLFIRINOX) (F), comparing with the untreated condition (dashed line). Colonospheres obtained are significantly more abundant in the F3 subpopulation compared to TP or F1 after 5-FU treatment for SW620 and T84 cell lines, after FOLFOX and FOLFIRINOX treatment for WiDr, and after FOLFIRI treatment for WiDr, SW480 and T84. All these results are represented as means ± SEM and statistical differences with *p-value < 0.05, **p-value < 0.01 and *alone for significant results compared to TP using One-way ANOVA test.

 doi:10.20944/preprints202205.0201.v1

Overall, these results confirm those obtained in 2D, the F3 subpopulation is predominantly the most resistant to monochemotherapy and chemotherapy combinations among the sorted cell subpopulations. Thus, in our study, we identified two therapeutically relevant cell subpopulations: the F1 subpopulation that seems to be chemosensitive while F3 is chemoresistant, from both early and advanced CRC cell lines. Our results show that this approach based on SdFFF cell sorting allows to identify chemoresistance. Cell lines may be distant from the heterogeneity and complexity of tumors. Therefore, we will test our approach using primary colorectal cancer cultures.

3.5. F3 subpopulation exhibits CSC-like features and chemoresistance in primary colorectal cancer cultures.

To confirm the promising results obtained from the cell lines, we performed the same experiments using CRC primary cultures. The primary culture CPP14 was established from an early stage CRC while CPP35 was derived from a tumor that had invaded the peritoneum i.e. at a more advanced stage, with the clinical data summarized in Table 1. As previously conducted on cell lines, the SdFFF-sorted cell subpopulations were characterized at the phenotypic and functional levels. Phenotypically, both primary cultures express CSC markers but with higher levels of LGR5 and BMI1 markers in CPP35 compared with CPP14 (Figure S3A). Interestingly, we noticed the same expression pattern of CD44 and BMI1 markers between CPP14 and early stage cell lines, and CD44, BMI1 and CD133 markers between CPP35 and late stage cell lines (Figure S3A). No significant differences in marker expression are observed between the sorted cell subpopulations (Figure S3A). Next, we investigated the cell cycle distribution of these two primary cultures. G0/G1 cells are significantly more abundant in F3 compared to the other subpopulations for CPP35, with a similar trend for CPP14 (Figure S3B). Conversely, the number of cells in G2/M is significantly lower in F3 compared to the other subpopulations for both primary cultures (Figure S3C). Afterwards, clonogenicity results showed that the F3 subpopulation forms significantly more and larger colonies than F1 for CPP14, with a similar trend for CPP35 (Figure S3D-E). Thus, two sorted cell subpopulations emerge from the primary culture characterization results: F1 and F3, with CSC features for F3 such as quiescence and clonogenicity. Hereafter, we will focus on F1 and F3 for chemosensitivity testing. These results are consistent with those obtained from cell lines, demonstrating the ability of SdFFF to sort cell subpopulations from both cell lines and primary cultures.

Subsequently, the response of these sorted cell subpopulations to chemotherapies was evaluated in 2D and 3D cell culture models for each primary culture. In 2D, we analyzed cell viability after 5-FU treatment, as well as induced proliferation and apoptosis (Figure 6A-C). No significant difference is observed between the IC50 values of the cell subpopulations (Figure 6A). After 5-FU treatment, the proliferation rate appears to be higher in the F3 subpopulation of CPP35 compared to F1 while 5-FU induced apoptosis is significantly higher in the F1 subpopulation compared to F3 for both primary cultures (Figure 6B-C). Thus, the F1 subpopulation seems to be more sensitive to 5-FU due to its susceptibility to apoptosis compared to TP and F3 in both primary cultures (Figure 6C). The oxaliplatin IC50s of both primary cultures are very slightly higher in the F3 subpopulation compared to F1 (Figure S4A). After oxaliplatin treatment, proliferation is significantly increased in F3 compared to TP for CPP35 and apoptosis seems to decrease in F3 versus F1 (Figure S4B-C). Similar findings are observed after treatment with irinotecan (Figure S4D-F). Hence, the F3 subpopulation appears to be more resistant to monochemotherapy than F1, due to a susceptibility of F1 to 5-FU-induced apoptosis and significant proliferation of F3 after oxaliplatin treatment.

Preprints (www.preprints.org) | NOT PEER-REVIEWED | Posted: 16 May 2022 doi:10.20944/preprints202205.0201.v1

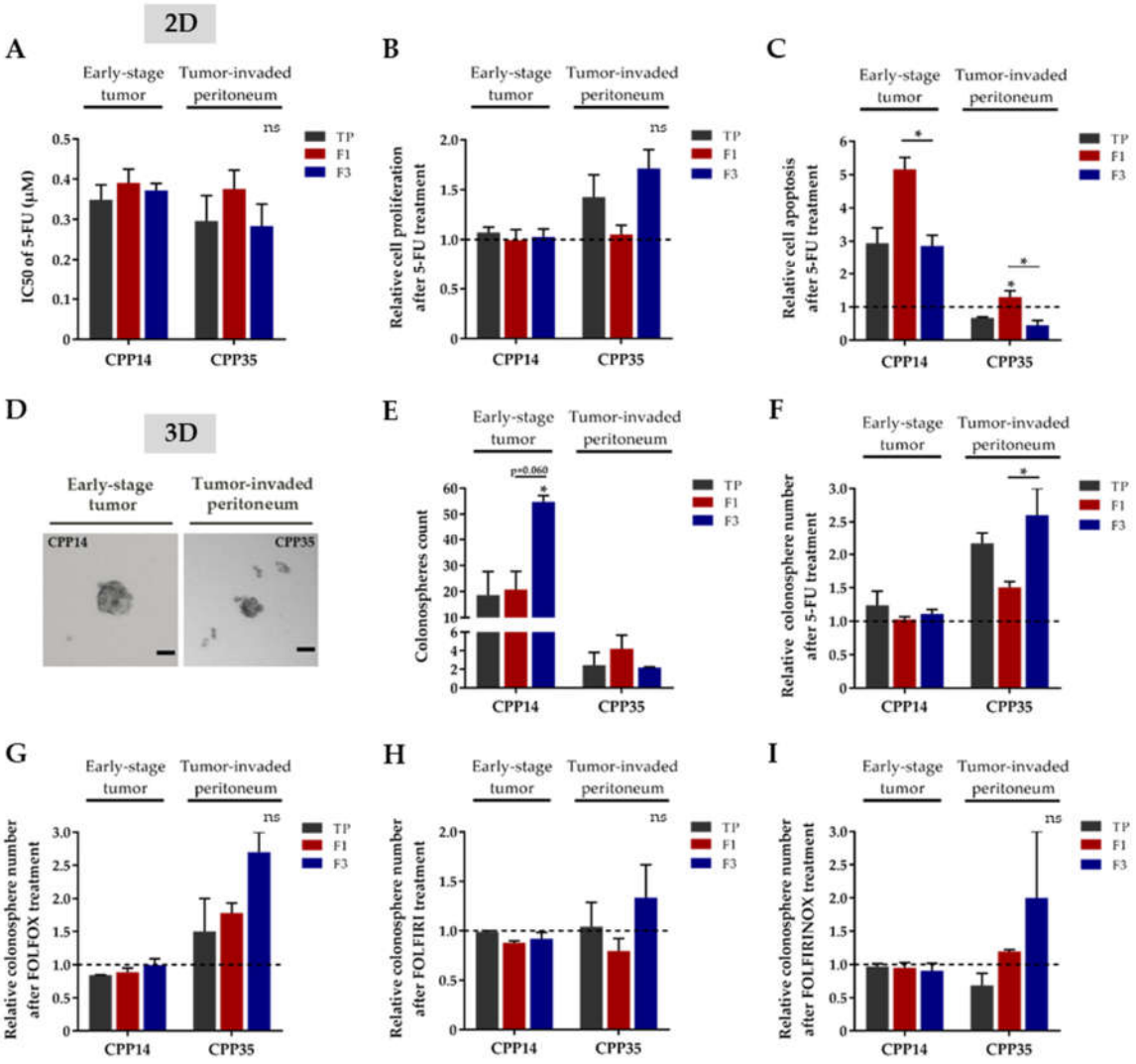

Figure 6. Chemoresistance of F3 subpopulation from both primary cultures. (A) The IC50 values obtained by the MTT assay show that the F1 subpopulation seems to have a slightly higher IC50 than the other cell subpopulations for the CPP35 primary culture. (B) After 5-FU treatment, cell proliferation assessed by BrdU assay appears to be enhanced for the F3 subpopulation compared to F1 and the untreated condition (dashed line) for CPP35. (C) Apoptosis rate analyzed by ELISA cell death assay is significantly decreased in F3 subpopulation compared to F1 for both primary cultures. (D) The tumorigenic potential of cells in vitro was evaluated by a sphere formation assay and showed that the colonospheres obtained from the two primary cultures had similar morphologies but different sizes. Scale bar 50 µm. (E) In untreated condition, F3 subpopulation has a significantly higher ability than F1 to form colonospheres for the CPP14 primary culture. (F-I) The impact of chemotherapies on CSC tumorigenic properties in vitro was investigated after treatment with 5-FU alone (F) or in combination: FOLFOX (G), FOLFIRI (H) or FOLFIRINOX (I). Colonospheres are significantly more abundant in F3 subpopulation after 5-FU treatment for CPP35, and the trend appears to be similar after FOLFOX, FOLFIRI, and FOLFIRINOX treatments. All these results are represented as means ± SEM and statistical differences with ns for not significant, *p-value < 0.05 and *alone for significant results compared to TP using One-way ANOVA test.

Finally, we investigated the response of SdFFF-sorted cell subpopulations in a 3D culture model to 5-FU alone or in combination with other chemotherapies. In the absence of treatment, both primary cultures have the ability to form colonospheres, but with a larger size for CPP14 (Figure 6D). Quantitatively, CPP14 forms more colonospheres than

 doi:10.20944/preprints202205.0201.v1

CPP35, with 18 and 2.5 colonospheres formed respectively when comparing TP values (Figure 6E). Remarkably, F3 generates significantly two-fold more colonospheres than the other cell subpopulations (Figure 6E). In the treated condition, the F3 subpopulation of CPP35 forms significantly more colonospheres than F1 after 5-FU treatment, with a similar trend after oxaliplatin and irinotecan treatment as well as chemotherapy combinations (Figure 6F-I and S4G-H). The significant difference in untreated condition between F1 and F3 of CPP14 could explain the minor differences observed in treated condition (Figure 6E-I). The colonosphere results are in agreement with those obtained for the cell lines, F3 is predominantly the most chemotherapy-resistant sorted cell subpopulation (Figure 4, 5 and 6). Therefore, our findings demonstrate that the study of the individualized response of each SdFFF-sorted cell subpopulation to chemotherapies is fully feasible from primary cultures.

4. Discussion

Our study addresses the impact of intratumoral cellular heterogeneity in the context of treatment resistance, without relying on surface marker expression for cell subpopulation sorting. Regardless of cell line and stage, the SdFFF technique allowed the isolation of three cell subpopulations based on their biophysical properties, with distinct phenotypic and functional characteristics. Compared to previous results [10], we show here the presence of two therapeutically relevant cell subpopulations based on CSCs characteristics: F1 and F3, thanks in particular to flow cytometry, in vivo tumor initiation assay and in vitro chemosensitivity tests. The F1 subpopulation is proliferative and chemosensitive, while the F3 subpopulation exhibits CSC functional hallmarks, especially the ability to initiate tumors in mice and chemoresistance. These two cell subpopulations of interest were identified from both early and late stage cell lines as well as from primary cultures. Therefore, using a label-free approach, we highlighted a cell subpopulation with a CSC-like phenotype that may play a crucial role in tumor progression and recurrence.

Initially identified in acute myeloid leukemia, CSCs were later discovered in many solid cancers such as CRC based on the expression of surface markers [22]. In CRC, early publications on CSCs used surface markers as a prerequisite to identify these cells [23–29]. Numerous CSC markers have been identified in CRC and are reviewed in Hervieu et al. [9]. Our phenotypic characterization results were initially underwhelming due to the lack of significant differences between the sorted cell subpopulations for three of the four cell lines studied although a trend did emerge. However, several publications have questioned the use of these markers because no CSC marker is 100% reliable as they are also expressed by intestinal stem cells and cancer cells [20,30,31]. Furthermore, Prasetyanti and Medema point out that CSC markers can be considered as a highly context-dependent property of cells [32]. Furthermore, the use of surface markers is hampered by the plasticity of CSCs, which is another obstacle to their identification and isolation. Both Shimokawa et al. and de Sousa e Melo et al. showed that ablation of $LGR5^+$ CSCs limits tumor growth but does not prevent tumor regrowth due to re-emergence of $LGR5^+$ CSCs from proliferating LGR5- cells [33,34]. Intriguingly, another study demonstrated that dissemination and metastatic colonization were carried out by $LGR5^-$ cells in CRC, with subsequent re-emergence of $LGR5^+$ CSCs at the metastatic site [7]. Thus, the ability of CSCs and non-CSCs to switch from one state to another, known as cellular plasticity, appears to be crucial for primary tumor growth and metastasis. These results highlight the complexity of identifying and especially isolating these CSCs due to shared expression with non-CSCs and cellular plasticity. Accumulating evidence points out that stemness is not as hierarchical and fixed as originally thought, but rather dynamic and endowed with considerable plasticity. Our label-free cell sorting approach, based on the biophysical properties of the cells, provides new insights to isolate CSC-enriched subpopulations.

A consensus has emerged suggesting that functional capabilities, particularly tumorigenic potential and chemoresistance, are more reliable for identifying CSCs than surface markers [35]. Surprisingly, our results show that cells with the ability to initiate tumors in

 doi:10.20944/preprints202205.0201.v1

mice and chemoresistance are not necessarily correlated with cells expressing CSC markers. The publication of Lenos et al. is in agreement with our observations, and demonstrates that there is a divergence between cells positive for CSC markers and cells with CSC functionality [36]. The previously proposed models of clonal evolution and CSCs are not mutually exclusive, and seem to be partly reconciled in the new emerging model: the plasticity model [32,37]. In the plasticity model, the conversion capacity is dynamic and bidirectional, from a non-CSC state to a CSC state and vice versa, and determined by various intrinsic and extrinsic signals such as the tumor microenvironment (TME) and therapy [32]. TME includes cancer and non-cancer cells including stromal cells, endothelial cells, immune cells and cancer-associated fibroblasts, as well as non-cellular components such as the extracellular matrix and cytokines. Accumulating evidence suggests that interaction and crosstalk within the TME can modulate the cellular state, stemness, plasticity, and many fundamental characteristics of CSC [32,37,38]. In our study, the in vivo tumor initiation assay results suggest cooperation of non-CSC cancer cells with CSCs. Indeed, we notice that for the control five mice carry tumors while the CSC-enriched subpopulation has only four, which may indicate that the presence of both CSCs and non-CSCs in TP promotes tumor development.

CSCs are particularly therapeutically attractive. Although chemotherapies eliminate most tumor cells, CSCs are able to escape the lethal effect of these drugs, which can lead to tumor recurrence. One of the main reasons for treatment failure is that anticancer drugs often only target actively cycling tumor cells and therefore do not affect CSCs, which are frequently in a quiescent or poorly proliferative state. Our study results support this explanation; the cell subpopulation enriched in CSC features is quiescent/poorly proliferative and chemoresistant, whereas the subpopulation of actively cycling cells is more sensitive. Similar findings were reported in Kreso et al. [39]. Remarkably, our study shows that only the CSC-enriched cell subpopulation escapes chemotherapy by significantly increasing treatment-induced cell proliferation without any change in cell death, demonstrating cell plasticity, as illustrated by the results obtained with the WiDr cell line in response to 5-FU-based chemotherapies in the 3D model. Furthermore, our results highlight that resistance and therapeutic escape are a functional property of CSCs, reinforcing the relevance of our approach based on label-free cell sorting by SdFFF. Collectively, our in vitro results reflect what frequently happens in CRC patients: chemotherapies kill proliferative cells, i.e. the F1 subpopulation, resulting in tumor regression, but fail to target CSCs, i.e. the F3 subpopulation, which are resistant and evade therapy leading to cancer relapse in patients. Therapies targeting CSCs are a promising therapeutic approach. However, the development of anticancer agents capable of specifically targeting CSCs has proven very difficult or has shown limited efficacy [40]. These disappointing results may be explained by the fact that the study models used often fail to recapitulate the patients' tumors [32]. One of our original hypotheses was that cell subpopulations isolated from early stage CRC cell lines might behave differently to chemotherapies than those from metastatic stages. Although one of the two metastatic cell lines had the highest IC50 for each of the chemotherapies tested, the results were not as pronounced as initially expected. Cancer cell lines grown in 2D have traditionally been used as a source to model cancer, but their inability to capture components of the microenvironment may impact response to treatment [32]. Cellular heterogeneity and plasticity may also compromise treatment efficacy, as highlighted in the studies of Shimokawa et al. and de Sousa e Melo et al. [32–34,38]. CRC patient-derived cultures, such as primary cultures, better model the heterogeneity and complexity of patient tumors, which are critical for treatment response. In our study, the IC50 differences are more pronounced between the two different stage primary cultures, especially for oxaliplatin and irinotecan, which may provide leads for more personalized therapy in patients from whom the primary cultures were derived. In addition to improving the biological material used, 3D cell culture models can improve chemotherapy response studies [32]. Our 3D chemosensitivity results from microtumor-

 doi:10.20944/preprints202205.0201.v1

like spheroids confirmed those obtained in 2D. Importantly, the CSC-enriched subpopulation sorted by SdFFF has the ability to survive in serum-free and suspension media, and to proliferate even in the presence of chemotherapy. Thus, cell proliferation plays a crucial role for this cell subpopulation sorted by SdFFF in response to stress such as chemotherapies. Therefore, our study models based on label-free cell sorting provide new insights to study responses to therapies and resistance mechanisms developed by CSCs. Nevertheless, the main components of TEM need to be integrated into our model in order to be as close as possible to the patients' tumors [32]. Future cancer therapies will need to consider both the CSCs and non-CSCs that form the tumor mass as well as the surrounding TEM.

In summary, we have demonstrated the relevance of our label-free approach to identify a chemoresistant cell subpopulation with CSC hallmarks. The signaling pathways associated with therapeutic resistance in the CSC-enriched subpopulation need to be further explored. This approach allows to unravel intratumoral cellular heterogeneity and to study in an individualized way the response to therapies of each cellular subpopulation of a biological tumor sample. Therefore, our findings open new perspectives for a deeper understanding of CSC-related resistance and, more importantly, provide leads for a more personalized therapy by identifying through our approach the responses to therapies of each tumor compartment.

Supplementary Materials: The following supporting information can be downloaded at: www.mdpi.com. Figure S1: Phenotypic and functional characterization of sedimentation field-flow fractionation (SdFFF)-sorted cell subpopulations from colorectal cancer (CRC) cell lines; Figure S2: Response of SdFFF-sorted cell subpopulations to oxaliplatin and irinotecan from CRC cell lines; Figure S3: Phenotypic and functional characterization of SdFFF-sorted cell subpopulations from CRC primary cultures; Figure S4: Response of SdFFF-sorted cell subpopulations to oxaliplatin and irinotecan from CRC primary cultures.

Author Contributions: Conceptualization, C.H., S.B. and M.M.; methodology, C.H., M.V., M.S., J.P., S.B. and M.M.; writing—original draft preparation, C.H.; writing—review and editing, C.H., M.V., G.B., N.C., M.S., J.P., S.B. and M.M. All authors have read and agreed to the published version of the manuscript.

Funding: This research was funded by the 'Comité Départemental de La Haute-Vienne de la Ligue Nationale Contre le Cancer', by the 'Comité d'Orientation de la Recherche en Cancérologie' (CORC) of Limoges and received a donation from the family of Mr Ballihi.

Institutional Review Board Statement: The animal study protocol was approved by the Ethics Committee for Animal Experimentation No. 33 and by the French Ministry of Higher Education, Research and Innovation (protocol code APAFIS#3 1963-2021061014298122 v2, approved July 21, 2021). The animal experimentation project was carried out within the user establishment: the animal facility located at the Faculty of Medicine and Pharmacy, University of Limoges (approval number B8708503).

Acknowledgments: We would like to thank the anticancer preparation unit of the Limoges University Hospital for the chemotherapies especially Dr Gaëlle Maillan, the animal facility of the BISCEM platform for their help during the in vivo experimentation, Alice Hémard for her help during her internship and the anatomo-pathology department of the Limoges University Hospital, in particular Sandrine Robert, Alain Chaunavel and Dr Aurélie Charissoux.

Conflicts of Interest: The authors declare no conflict of interest. The funders had no role in the design of the study; in the collection, analyses, or interpretation of data; in the writing of the manuscript, or in the decision to publish the results.

References

1. Siegel, R.L.; Miller, K.D.; Fuchs, H.E.; Jemal, A. Cancer Statistics, 2022. *CA. Cancer J. Clin.* **2022**, *72*, 7–33, doi:10.3322/caac.21708.

2. Dekker, E.; Tanis, P.J.; Vleugels, J.L.A.; Kasi, P.M.; Wallace, M.B. Colorectal Cancer. *The Lancet* **2019**, *394*, 1467–1480, doi:10.1016/S0140-6736(19)32319-0.

3. Labianca, R.; Nordlinger, B.; Beretta, G.D.; Mosconi, S.; Mandalà, M.; Cervantes, A.; Arnold, D. Early Colon Cancer: ESMO Clinical Practice Guidelines for Diagnosis, Treatment and Follow-Up. *Ann. Oncol.* **2013**, *24*, vi64–vi72, doi:10.1093/annonc/mdt354.

4. Van Cutsem, E.; Cervantes, A.; Adam, R.; Sobrero, A.; Van Krieken, J.H.; Aderka, D.; Aranda Aguilar, E.; Bardelli, A.; Benson, A.; Bodoky, G.; et al. ESMO Consensus Guidelines for the Management of Patients with Metastatic Colorectal Cancer. *Ann. Oncol.* **2016**, *27*, 1386–1422, doi:10.1093/annonc/mdw235.

5. van der Heijden, M.; Vermeulen, L. Stem Cells in Homeostasis and Cancer of the Gut. *Mol. Cancer* **2019**, *18*, 66, doi:10.1186/s12943-019-0962-x.

6. Relier, S.; Ripoll, J.; Guillorit, H.; Amalric, A.; Achour, C.; Boissière, F.; Vialaret, J.; Attina, A.; Debart, F.; Choquet, A.; et al. FTO-Mediated Cytoplasmic M6Am Demethylation Adjusts Stem-like Properties in Colorectal Cancer Cell. *Nat. Commun.* **2021**, *12*, 1716, doi:10.1038/s41467-021-21758-4.

7. Fumagalli, A.; Oost, K.C.; Kester, L.; Morgner, J.; Bornes, L.; Bruens, L.; Spaargaren, L.; Azkanaz, M.; Schelfhorst, T.; Beerling, E.; et al. Plasticity of Lgr5-Negative Cancer Cells Drives Metastasis in Colorectal Cancer. *Cell Stem Cell* **2020**, *26*, 569-578.e7, doi:10.1016/j.stem.2020.02.008.

8. Morral, C.; Stanisavljevic, J.; Hernando-Momblona, X.; Mereu, E.; Álvarez-Varela, A.; Cortina, C.; Stork, D.; Slebe, F.; Turon, G.; Whissell, G.; et al. Zonation of Ribosomal DNA Transcription Defines a Stem Cell Hierarchy in Colorectal Cancer. *Cell Stem Cell* **2020**, *26*, 845-861.e12, doi:10.1016/j.stem.2020.04.012.

9. Hervieu, C.; Christou, N.; Battu, S.; Mathonnet, M. The Role of Cancer Stem Cells in Colorectal Cancer: From the Basics to Novel Clinical Trials. *Cancers* **2021**, *13*, 1092, doi:10.3390/cancers13051092.

10. Mélin, C.; Perraud, A.; Akil, H.; Jauberteau, M.-O.; Cardot, P.; Mathonnet, M.; Battu, S. Cancer Stem Cell Sorting from Colorectal Cancer Cell Lines by Sedimentation Field Flow Fractionation. *Anal. Chem.* **2012**, *84*, 1549–1556, doi:10.1021/ac202797z.

11. Mélin, C.; Lacroix, A.; Lalloué, F.; Pothier, A.; Zhang, L.Y.; Perraud, A.; Dalmay, C.; Lautrette, C.; Jauberteau, M.-O.; Cardot, P.; et al. Improved Sedimentation Field-Flow Fractionation Separation Channel for Concentrated Cellular Elution. *J. Chromatogr. A* **2013**, *1302*, 118–124, doi:10.1016/j.chroma.2013.05.067.

12. Mélin, C.; Perraud, A.; Christou, N.; Bibes, R.; Cardot, P.; Jauberteau, M.-O.; Battu, S.; Mathonnet, M. New Ex-Ovo Colorectal-Cancer Models from Different SdFFF-Sorted Tumor-Initiating Cells. *Anal. Bioanal. Chem.* **2015**, *407*, 8433–8443, doi:10.1007/s00216-015-9029-z.

13. Akil, H.; Perraud, A.; Mélin, C.; Jauberteau, M.-O.; Mathonnet, M. Fine-Tuning Roles of Endogenous Brain-Derived Neurotrophic Factor, TrkB and Sortilin in Colorectal Cancer Cell Survival. *PLoS ONE* **2011**, *6*, e25097, doi:10.1371/journal.pone.0025097.

14. Amin, M.B.; Edge, S.; Greene, F.; Byrd, D.R.; Brookland, R.K.; Washington, M.K.; Gershenwald, J.E.; Compton, C.C.; Hess, K.R.; Sullivan, D.C.; et al. AJCC Cancer Staging Manual - 8th Edition 2017.

15. Bégaud-Grimaud, G.; Battu, S.; Leger, D.; Cardot, P.J.P. Mammalian Cell Sorting with Sedimentation Field-Flow Fractionation. In *Field-Flow Fractionation in Biopolymer Analysis*; Williams, S.K.R., Caldwell, K.D., Eds.; Springer Vienna: Vienna, 2012; pp. 223–253 ISBN 978-3-7091-0153-7.

16. Hu, Y.; Smyth, G.K. ELDA: Extreme Limiting Dilution Analysis for Comparing Depleted and Enriched Populations in Stem Cell and Other Assays. *J. Immunol. Methods* **2009**, *347*, 70–78, doi:10.1016/j.jim.2009.06.008.

17. Giraud, J.; Molina-Castro, S.; Seeneevassen, L.; Sifré, E.; Izotte, J.; Tiffon, C.; Staedel, C.; Boeuf, H.; Fernandez, S.; Barthelemy, P.; et al. Verteporfin Targeting YAP1/TAZ-TEAD Transcriptional Activity Inhibits the Tumorigenic Properties of Gastric Cancer Stem Cells. *Int. J. Cancer* **2020**, *146*, 2255–2267, doi:10.1002/ijc.32667.

18. Relier, S.; Yazdani, L.; Ayad, O.; Choquet, A.; Bourgaux, J.-F.; Prudhomme, M.; Pannequin, J.; Macari, F.; David, A. Antibiotics Inhibit Sphere-Forming Ability in Suspension Culture. *Cancer Cell Int.* **2016**, *16*, 6, doi:10.1186/s12935-016-0277-6.

19. Mélin, C.; Perraud, A.; Bounaix Morand du Puch, C.; Loum, E.; Giraud, S.; Cardot, P.; Jauberteau, M.-O.; Lautrette, C.; Battu, S.; Mathonnet, M. Sedimentation Field Flow Fractionation Monitoring of in Vitro Enrichment in Cancer Stem Cells by Specific Serum-Free Culture Medium. *J. Chromatogr. B* **2014**, *963*, 40–46, doi:10.1016/j.jchromb.2014.05.039.

20. Puglisi, M.A. Colon Cancer Stem Cells: Controversies and Perspectives. *World J. Gastroenterol.* **2013**, *19*, 2997, doi:10.3748/wjg.v19.i20.2997.

21. Yang, W.; Soares, J.; Greninger, P.; Edelman, E.J.; Lightfoot, H.; Forbes, S.; Bindal, N.; Beare, D.; Smith, J.A.; Thompson, I.R.; et al. Genomics of Drug Sensitivity in Cancer (GDSC): A Resource for Therapeutic Biomarker Discovery in Cancer Cells. *Nucleic Acids Res.* **2012**, *41*, D955–D961, doi:10.1093/nar/gks1111.

22. Bonnet, D.; Dick, J.E. Human Acute Myeloid Leukemia Is Organized as a Hierarchy That Originates from a Primitive Hematopoietic Cell. *Nat. Med.* **1997**.

23. Ricci-Vitiani, L.; Lombardi, D.G.; Pilozzi, E.; Biffoni, M.; Todaro, M.; Peschle, C.; De Maria, R. Identification and Expansion of Human Colon-Cancer-Initiating Cells. *Nature* **2007**, *445*, 111–115, doi:10.1038/nature05384.

24. O'Brien, C.A.; Pollett, A.; Gallinger, S.; Dick, J.E. A Human Colon Cancer Cell Capable of Initiating Tumour Growth in Immunodeficient Mice. *Nature* **2007**, *445*, 106–110, doi:10.1038/nature05372.

25. Dalerba, P.; Dylla, S.J.; Park, I.-K.; Liu, R.; Wang, X.; Cho, R.W.; Hoey, T.; Gurney, A.; Huang, E.H.; Simeone, D.M.; et al. Phenotypic Characterization of Human Colorectal Cancer Stem Cells. *Proc. Natl. Acad. Sci.* **2007**, *104*, 10158–10163, doi:10.1073/pnas.0703478104.

26. Barker, N.; van Es, J.H.; Kuipers, J.; Kujala, P.; van den Born, M.; Cozijnsen, M.; Haegebarth, A.; Korving, J.; Begthel, H.; Peters, P.J.; et al. Identification of Stem Cells in Small Intestine and Colon by Marker Gene Lgr5. *Nature* **2007**, *449*, 1003–1007, doi:10.1038/nature06196.

27. Barker, N.; Ridgway, R.A.; van Es, J.H.; van de Wetering, M.; Begthel, H.; van den Born, M.; Danenberg, E.; Clarke, A.R.; Sansom, O.J.; Clevers, H. Crypt Stem Cells as the Cells-of-Origin of Intestinal Cancer. *Nature* **2009**, *457*, 608–611, doi:10.1038/nature07602.

28. Sangiorgi, E.; Capecchi, M.R. Bmi1 Is Expressed in Vivo in Intestinal Stem Cells. *Nat. Genet.* **2008**, *40*, 915–920, doi:10.1038/ng.165.

29. Vermeulen, L.; Todaro, M.; de Sousa Mello, F.; Sprick, M.R.; Kemper, K.; Perez Alea, M.; Richel, D.J.; Stassi, G.; Medema, J.P. Single-Cell Cloning of Colon Cancer Stem Cells Reveals a Multi-Lineage Differentiation Capacity. *Proc. Natl. Acad. Sci.* **2008**, *105*, 13427–13432, doi:10.1073/pnas.0805706105.

30. Shmelkov, S.V.; Butler, J.M.; Hooper, A.T.; Hormigo, A.; Kushner, J.; Milde, T.; St. Clair, R.; Baljevic, M.; White, I.; Jin, D.K.; et al. CD133 Expression Is Not Restricted to Stem Cells, and Both CD133+ and CD133– Metastatic Colon Cancer Cells Initiate Tumors. *J. Clin. Invest.* **2008**, JCI34401, doi:10.1172/JCI34401.

31. Jahanafrooz, Z.; Mosafer, J.; Akbari, M.; Hashemzaei, M.; Mokhtarzadeh, A.; Baradaran, B. Colon Cancer Therapy by Focusing on Colon Cancer Stem Cells and Their Tumor Microenvironment. *J. Cell. Physiol.* **2020**, *235*, 4153–4166, doi:10.1002/jcp.29337.

32. Prasetyanti, P.R.; Medema, J.P. Intra-Tumor Heterogeneity from a Cancer Stem Cell Perspective. *Mol. Cancer* **2017**, *16*, 41, doi:10.1186/s12943-017-0600-4.

33. Shimokawa, M.; Ohta, Y.; Nishikori, S.; Matano, M.; Takano, A.; Fujii, M.; Date, S.; Sugimoto, S.; Kanai, T.; Sato, T. Visualization and Targeting of LGR5+ Human Colon Cancer Stem Cells. *Nature* **2017**, *545*, 187–192, doi:10.1038/nature22081.

34. de Sousa e Melo, F.; Kurtova, A.V.; Harnoss, J.M.; Kljavin, N.; Hoeck, J.D.; Hung, J.; Anderson, J.E.; Storm, E.E.; Modrusan, Z.; Koeppen, H.; et al. A Distinct Role for Lgr5+ Stem Cells in Primary and Metastatic Colon Cancer. *Nature* **2017**, *543*, 676–680, doi:10.1038/nature21713.

35. Visvader, J.E.; Lindeman, G.J. Cancer Stem Cells: Current Status and Evolving Complexities. *Cell Stem Cell* **2012**, *10*, 717–728, doi:10.1016/j.stem.2012.05.007.

36. Lenos, K.J.; Miedema, D.M.; Lodestijn, S.C.; Nijman, L.E.; van den Bosch, T.; Romero Ros, X.; Lourenço, F.C.; Lecca, M.C.; van der Heijden, M.; van Neerven, S.M.; et al. Stem Cell Functionality Is Microenvironmentally Defined during Tumour Expansion and Therapy Response in Colon Cancer. *Nat. Cell Biol.* **2018**, *20*, 1193–1202, doi:10.1038/s41556-018-0179-z.

37. Thankamony, A.P.; Saxena, K.; Murali, R.; Jolly, M.K.; Nair, R. Cancer Stem Cell Plasticity – A Deadly Deal. *Front. Mol. Biosci.* **2020**, *7*, 79, doi:10.3389/fmolb.2020.00079.

38. Zheng, X.; Yu, C.; Xu, M. Linking Tumor Microenvironment to Plasticity of Cancer Stem Cells: Mechanisms and Application in Cancer Therapy. *Front. Oncol.* **2021**, *11*, 678333, doi:10.3389/fonc.2021.678333.

39. Kreso, A.; O'Brien, C.A.; van Galen, P.; Gan, O.I.; Notta, F.; Brown, A.M.K.; Ng, K.; Ma, J.; Wienholds, E.; Dunant, C.; et al. Variable Clonal Repopulation Dynamics Influence Chemotherapy Response in Colorectal Cancer. *Science* **2013**, *339*, 543–548, doi:10.1126/science.1227670.

40. de Sousa e Melo, F.; de Sauvage, F.J. Cellular Plasticity in Intestinal Homeostasis and Disease. *Cell Stem Cell* **2019**, *24*, 54–64, doi:10.1016/j.stem.2018.11.019.